

SCIENTIFIC REPORTS



OPEN

Coexistence of topological Dirac fermions on the surface and three-dimensional Dirac cone state in the bulk of ZrTe_5 single crystal

Arnab Pariari & Prabhat Mandal

Received: 26 August 2016
Accepted: 02 December 2016
Published: 09 January 2017

Although, the long-standing debate on the resistivity anomaly in ZrTe_5 somewhat comes to an end, the exact topological nature of the electronic band structure remains elusive till today. Theoretical calculations predicted that bulk ZrTe_5 to be either a weak or a strong three-dimensional (3D) topological insulator. However, the angle resolved photoemission spectroscopy and transport measurements clearly demonstrate 3D Dirac cone state with a small mass gap between the valence band and conduction band in the bulk. From the magnetization and magneto-transport measurements on ZrTe_5 single crystal, we have detected both the signature of helical spin texture from topological surface state and chiral anomaly associated with the 3D Dirac cone state in the bulk. This implies that ZrTe_5 hosts a novel electronic phase of material, having massless Dirac fermionic excitation in its bulk gap state, unlike earlier reported 3D topological insulators. Apart from the band topology, it is also apparent from the resistivity and Hall measurements that the anomalous peak in the resistivity can be shifted to a much lower temperature ($T < 2$ K) by controlling impurity and defects.

The low-dimensional pentatellurides, ZrTe_5 and HfTe_5 , synthesized in 1973¹, exhibit a peak in the resistivity (ρ) as a function of temperature². This anomaly in the resistivity has been observed at $T_p \sim 145$ K for ZrTe_5 and $T_p \sim 80$ K for HfTe_5 , however, the exact temperature varies from sample to sample depending on the impurity level³. With decreasing impurity, the anomalous peak in resistivity shifts to lower temperature³. Recent works on ZrTe_5 reported T_p as low as ~ 60 K, which has been ascribed to very low defect and impurity concentration in the samples^{4,5}. Most of the earlier works have been directed towards understanding the origin of this peak. The charge carrier switches from holes at $T > T_p$ to electrons for $T < T_p$, which is reflected in the sign change of thermoelectric power⁶ and Hall coefficient⁷. Initially, it was believed that this resistive anomaly arises due to a charge-density wave transition, similar to that occurs in NbSe_3 ⁸. But the absence of lattice modulation, etc., eliminate the idea of charge density wave formation in ZrTe_5 ⁹. Subsequently, the concept of polaronic conduction¹⁰, semimetal-semiconductor phase transition¹¹ and so on, have emerged until a recent theoretical work suggests that the monolayer of ZrTe_5 and HfTe_5 is the most promising candidate for the quantum spin Hall due to the large bulk gap¹². Suddenly, a material known for its large thermoelectric power⁶, resistivity anomaly¹ and large positive magnetoresistance¹³, has been brought to our attention to study the topological properties of relativistic Dirac fermion in condensed matter physics^{4,5,14–21}.

It has been established from the recent angle resolved photoelectron spectroscopy (ARPES) measurement that the temperature dependence of the electronic band structure across the Fermi energy is responsible for the anomalous peak in resistivity¹⁴. However, ZrTe_5 is not free from debate, facing a bigger question. Theoretical calculation shows that electronic band topology of bulk ZrTe_5 is very sensitive to the lattice parameters. Depending on the values of lattice parameters it can be either a weak or a strong three-dimensional topological insulator¹². On the other hand, ARPES^{4,14}, infrared spectroscopy^{5,15} and magneto transport⁴ studies show three-dimensional linear dispersion with a small semiconducting gap between the valence and conduction band, i.e., 3D Dirac fermionic excitation with a small mass gap. Do theory and experiment contradict each other or the topological Dirac fermions on the surface and three-dimensional Dirac cone state in the bulk can coexist simultaneously in ZrTe_5 ? If the

Saha Institute of Nuclear Physics, HBNI, 1/AF Bidhannagar, Calcutta 700 064, India. Correspondence and requests for materials should be addressed to P.M. (email: prabhat.mandal@saha.ac.in)

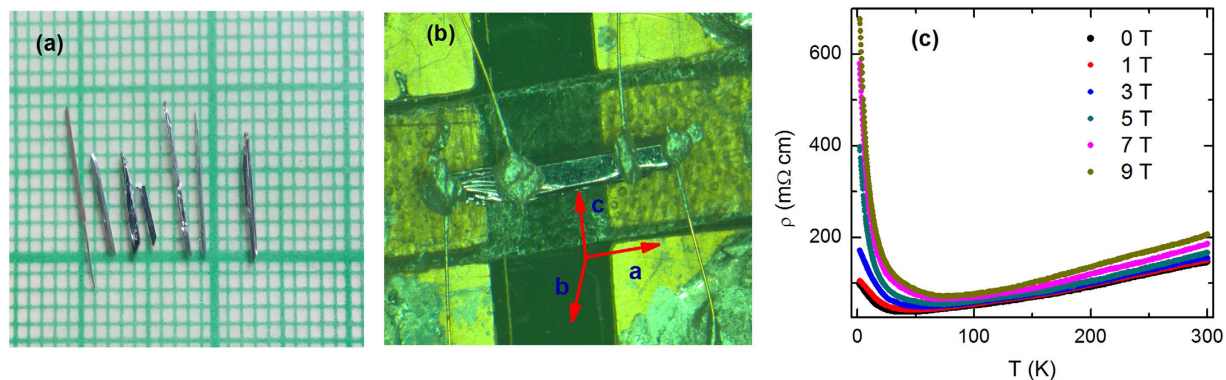


Figure 1. (a) Typical size and morphology of few representative single crystals of ZrTe_5 , (b) Different crystallographic directions, and (c) Temperature dependence of resistivity (ρ) both in presence and absence of external magnetic field.

later is possible, it would be a remarkable phenomenon. We will have a three-dimensional topological insulator with Dirac fermionic excitation in its bulk.

Results

Crystal structure. High quality single crystals of ZrTe_5 were grown by iodine vapor transport method similar to that reported earlier²². Typical size and morphology of few representative single crystals are shown in Fig. 1(a). Phase purity and the structural analysis of the samples were done by high resolution powder x-ray diffraction (XRD) technique (Rigaku, TTRAX II) using $\text{Cu-K}\alpha$ radiation [see Supplementary Figure S1]. Within the resolution of XRD, we have not seen any peak due to the impurity phase. The calculated value of the lattice parameters are $a = 3.96 \text{ \AA}$, $b = 14.50 \text{ \AA}$ and $c = 13.78 \text{ \AA}$ with space group symmetry $Cmcm$, similar to the earlier reports^{23–25}. The structure of the pentatellurides consists of trigonal prismatic chains of ZrTe_3 along a axis connected via parallel zigzag chains of Te atoms along the c axis, which together form 2D planes weakly bonded via van der Waals force along the b axis¹². Figure 1(b) shows the crystallographic directions of a typical ZrTe_5 single crystal.

Temperature dependence of resistivity both in presence and absence of external magnetic field.

Resistivity and transverse magnetoresistance measurements are done by applying current along the a axis and magnetic field perpendicular to the ac plane, i.e., along b axis. Figure 1(c) shows the temperature dependence of resistivity of ZrTe_5 single crystal both in presence and absence of magnetic field. The zero-field ρ exhibits metallic behavior ($d\rho/dT > 0$) down to 25 K. Below 25 K, ρ shows a weak upturn, i.e., a crossover from metallic to semiconducting like behavior. However, several earlier reports show that a broad peak appears in the temperature dependence of ρ , which is known as the resistivity anomaly of ZrTe_5 ^{1–5}. We have already mentioned that the temperature at which ρ shows peak varies widely; from 60 K to 170 K depending on the presence of impurity and defect concentration in the sample. It has been argued that the binding energy shift of the valence and conduction bands as a function of temperature is responsible for the peak at T_p ¹⁴. The sign of the charge carrier changes from positive (hole) to negative (electron) and the peak in $\rho(T)$ appears when the chemical potential crosses the gap ($\sim 50 \pm 10 \text{ meV}$) from valence band to conduction band. The absence of resistivity peak down to 2 K in the present sample could be attributed to much smaller impurities and defects. Under application of magnetic field, ρ increases sharply at low temperature and the metal-semiconductor crossover shifts to higher temperature, which are consistent with the earlier reports^{4,25}. But, no re-entrant metallic state has been observed up to 9 T.

Hall resistivity and transverse magnetoresistance. To further ensure the absence of resistivity anomaly, which has been ascribed to the switching of *p*-type semimetal to *n*-type semimetal state, we have done Hall measurements down to 2 K. Figure 2(a) shows that the Hall resistivity (ρ_{xy}) remains positive over the entire temperature range 2–300 K. The absence of sign change in ρ_{xy} is consistent with the observed *T* dependence of ρ . One can see that ρ_{xy} is linear over the entire field range except at low temperature, where an upward curvature appears at high fields due to the Shubnikov-de Haas oscillations. A systematic increase of the slope of the Hall resistivity with decreasing temperature is consistent with the temperature evolution of electronic band structure in ZrTe_5 ^{14,21}. From the slope of $\rho_{xy}(H)$, the bulk carrier density (*n*) is calculated to be $\sim 4 \times 10^{16} \text{ cm}^{-3}$ and $\sim 7 \times 10^{16} \text{ cm}^{-3}$ at 2 and 300 K, respectively. We would like to mention that the carrier density in the present crystal is almost one order of magnitude smaller than the earlier reported ones^{18,26}. Figure 2(b) shows the normalized magnetoresistance (MR) up to 9 T magnetic field. MR is large, positive and shows no sign of saturation in the measured temperature and field range. The observed behavior of MR is similar to the earlier reports^{13,16,17}. At low temperature, MR is dominated by a very low frequency ($\sim 3 \text{ T}$) Shubnikov-de Haas oscillation, which implies the presence of a tiny Fermi pocket, consistent with the low carrier density determined from the Hall measurements. Employing the Onsager relation $F = (\phi_0/2\pi^2)A_F$, we have calculated the cross-sectional area (A_F) of the Fermi

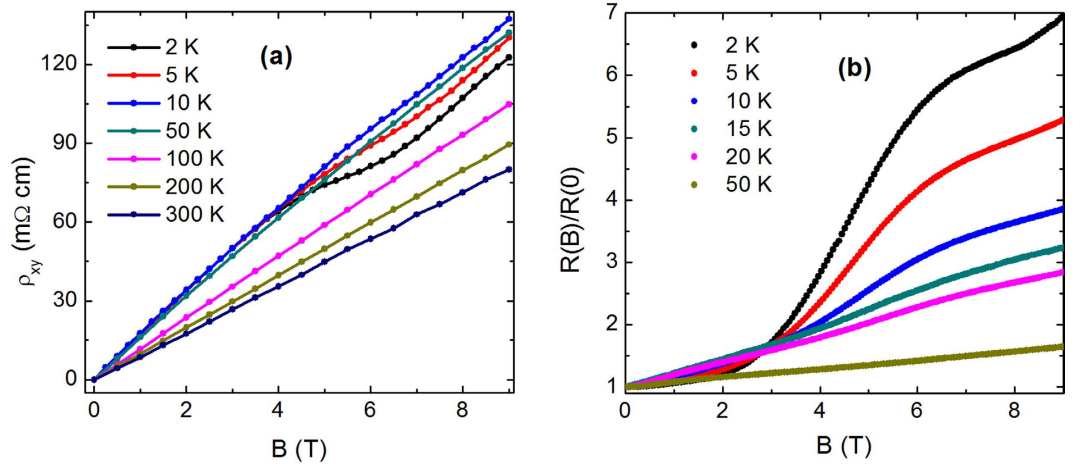


Figure 2. (a) Hall resistivity (ρ_{xy}) of ZrTe₅ single crystal at several representative temperatures over the range 2–300 K. (b) Transverse magnetoresistance ($I \perp \vec{B}$) normalized to the zero field value up to 9 T.

surface normal to the field $\sim 6.2 \times 10^{-5} \text{ \AA}^{-2}$. At high temperature, where the quantum oscillation suppresses, MR becomes linear.

Longitudinal magnetoresistance and Chiral anomaly. As proposed by Hermann Weyl in 1929, the four-component massless Dirac equation in three spatial dimensions can be separated into two two-component equations, $i \frac{\partial \Psi}{\partial t} = \pm c \vec{\sigma} \cdot \vec{p} \Psi$, where $\vec{\sigma}$ and \vec{p} are the Pauli matrices and momentum respectively. The above equation describes particles with a definite chirality $\vec{\sigma} \cdot \hat{p}$, known as Weyl fermions. according to the classical equation of motion the number of fermions with plus or minus chirality is conserved separately. But, the relativistic theory of charged chiral fermions in three spatial dimensions holds the so-called chiral anomaly- non-conservation of chiral charge induced by external gauge fields with non-trivial topology, known as Adler-Bell-Jackiw anomaly^{27,28}. Nielsen and Ninomiya provided a physical picture of the chiral anomaly in the context of condensed matter physics²⁹. Considering a band structure in three-dimension which supports two Weyl nodes with opposite chirality separated in momentum space and applying a magnetic field along the line joining the Weyl nodes, they predicted an enhanced magneto-conductance due to the charge pumping from one node to another in presence of an electric field (\vec{E}) parallel to \vec{B} .

In 3D Dirac semimetals, a four-component massless Dirac fermion is nothing but the two copies of distinct Weyl fermions. The application of magnetic field splits the four-fold degenerate Dirac node into two Weyl nodes of opposite chirality, along the direction of magnetic field^{30,31}. Initially, the plus and minus chirality fermions in the different Weyl nodes have same chemical potential $\mu^+ = \mu^-$. Whereas, \vec{E} parallel to \vec{B} creates an imbalance ($\mu^+ \neq \mu^-$) between the two Weyl nodes with opposite chirality, which induces a charge pumping from one Weyl node to another. The net current generation due to the chiral imbalance is $j_c = \frac{e^2 B}{4\pi^2 \hbar^2 c} (\mu^+ - \mu^-)^4$ ³¹. Again, ($\mu^+ - \mu^-$) is proportional to $\vec{E} \cdot \vec{B}$. As a result, the enhanced magneto-conductance is expected to show quadratic B dependence in the form, $\sigma_c = \sigma_0 + a(T) \cdot B^2$, where σ_0 is the zero-field conductivity. The field independent constant, $a(T)$ has the inverse T^2 dependence,

$$a(T) = \frac{e^2}{\pi \hbar} \frac{3 e^2 \nu^2}{8 \hbar c \pi^3} \frac{\tau_v}{T^2 + \frac{\mu^2}{\pi^2}}, \quad (1)$$

where ν , τ_v , and μ are the Fermi velocity, chirality changing scattering time and chemical potential, respectively⁴. But, in addition to the negative quadratic MR associated to chiral anomaly, small positive MR components associated to different physical phenomenon may contribute to transport^{32–34}. Conventional nonlinear band contribution around the Fermi level, which has the field dependence, $\sigma_N = \frac{1}{\rho_0 + A \cdot B^2}$, is common^{32–34}. As a result, the longitudinal magneto-conductance can be fitted with the theoretical expression, $\sigma = \sigma_c + \sigma_N = [\sigma_0 + a(T) \cdot B^2] + \frac{1}{\rho_0 + A \cdot B^2}$.

To probe the chiral anomaly, we have measured longitudinal magnetoresistance (LMR) by applying both the current and magnetic field along the **a** axis. As shown in Fig. 3(a), the resistance at 10 K gradually decreases with increasing field until an upturn occurs at high field. A small positive transverse MR component due to unavoidable misalignment in parallel configuration is responsible for this high field upturn. As the positive MR component rapidly suppresses with increasing temperature, the longitudinal negative MR becomes more clearly visible at higher temperatures. LMR at several other temperatures from 5 to 40 K, has been shown in Supplementary Figure S2. With further increase in temperature above 40 K, however, the negative MR itself becomes very weak. The negative LMR was reproduced by several independent measurements and also verified in different crystals. Chiral anomaly induced negative LMR has also been observed in earlier magneto-transport studies in ZrTe₅^{4,34}.

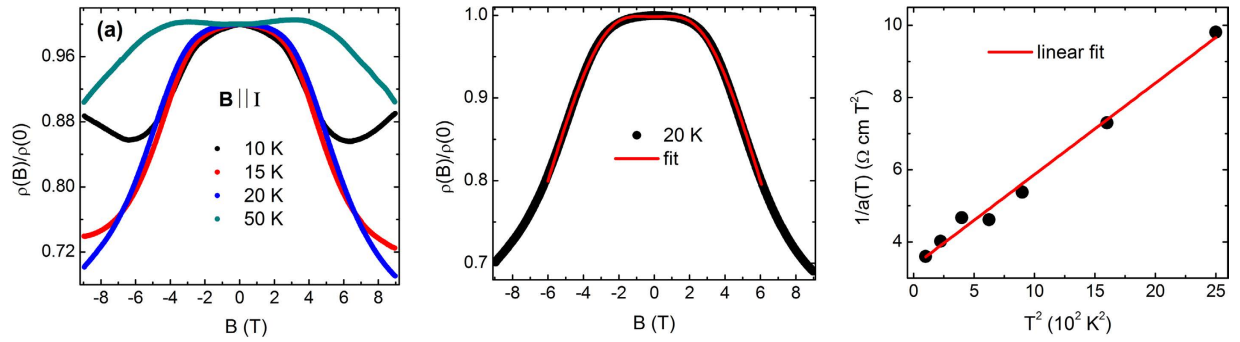


Figure 3. (a) Magnetoresistance measured at temperatures from 10 to 50 K, when applied current and magnetic field are parallel to each other, (b) Magnetoresistance at 20 K, fitted with the theoretical expression, $\rho_c = \frac{1}{[\sigma_0 + a(T) \cdot B^2] + \frac{1}{\rho_0 + A \cdot B^2}}$, and (c) Temperature dependence of $1/a$, where a is in the units of $\text{S cm}^{-1} \text{T}^{-2}$.

The nature and strength of negative LMR in the present sample are comparable to that reported earlier^{4,34}. LMR has been fitted with the inverse of the above mentioned theoretical expression for the longitudinal magneto-conductance and shown at a temperature 20 K in Fig. 3(b). A good fitting between the theoretical expression and experimental data is reflected in the above mentioned figure. By fitting LMR at different temperatures in the range 10–50 K [see Supplementary Figure S2 for the theoretical fitting at several representative temperatures], we have calculated the values of the parameter a . Observed value of $a(T)$ indicates that the strength of induced chiral current for the present sample is comparable with the earlier report on ZrTe_5 ⁴. In Fig. 3(c), we have plotted a^{-1} vs T^2 . One can see from the figure that a^{-1} is almost linear in T^2 , as predicted theoretically. Thus, the negative longitudinal MR in $\vec{E} \parallel \vec{B}$ configuration implies four-component massless Dirac fermionic excitation in the bulk state of ZrTe_5 single crystal^{4,34}. It may be noted that the negative MR due to induced chiral anomaly is a well established phenomenon in three-dimensional Dirac semimetals, which has also been observed in Cd_3As_2 ³¹ and Na_3Bi ³⁵. Presence of a small gap between the upper and lower Dirac cone in bulk may reduce the magnitude of the chiral current, but cannot destroy it fully⁴.

Signature of topological surface state from magnetization measurements. The low-energy physics of the surface state for a three-dimensional topological insulator can be described by the Dirac type effective Hamiltonian, $H_{\text{surf}}(k_x, k_y) = \hbar v_F (\sigma^x k_y - \sigma^y k_x)$, where v_F is the Fermi velocity^{36,37}. Thus, for a fixed translational momentum \vec{k} , the “spin”, denoted by the Pauli matrix $\vec{\sigma}$, has a fixed direction for the eigenstate of the Hamiltonian. This is the most important property of the nontrivial topological surface state in 3D topological insulators, known as “spin-momentum locking”. As the “spin” is always perpendicular to the momentum, one can introduce a helicity operator for the spin texture on circular constant energy contour of the Dirac cones³⁷, $\hat{h} = (1/k)\hat{z} \cdot (\vec{k} \times \vec{\sigma})$. This leads to left-handed spin texture for the upper Dirac cone and right-handed spin texture for the lower Dirac cone in the momentum space. Whereas at the Dirac point, as long as the Dirac spectrum is not gapped, the electron spin should be free to align along the applied magnetic field due to the singularity in spin orientation³⁸. This predicts a low-field paramagnetic peak in the susceptibility curve $\chi(H)$.

Figure 4(a) shows the magnetization of single crystal of ZrTe_5 with magnetic field along the a axis. Over the whole range of temperature from 2 to 350 K, ZrTe_5 shows diamagnetic signal except a paramagnetic upturn in the low-field region. It might be worthy to mention that single crystals of standard diamagnetic bismuth and three-dimensional Dirac semimetal Cd_3As_2 do not show this type of behaviour [see Supplementary Figure S3 and Figure S4(b)]. On the other hand, similar paramagnetic response has been observed in single crystals of well established three-dimensional topological insulator $\text{Bi}_{1.5}\text{Sb}_{0.5}\text{Te}_{1.7}\text{Se}_{1.3}$ [see Supplementary Figure S5]. Figure 4(b) shows that a cusp-like paramagnetic susceptibility sharply rises above the diamagnetic floor in a narrow field range of ~ 2 kOe around zero field. The height of the peak from the diamagnetic floor and its sharpness are insensitive to the temperature. This singular response of susceptibility shows no sign of thermal rounding up to as high as 350 K (~ 32 meV), which is almost one-half of the bulk band gap^{4,21}. Similar robust and singular paramagnetic response have been reported for the family of three-dimensional topological insulators which is the fingerprint of the helical spin texture of the topological Dirac fermions on the surface^{38,39}. Setting both the chemical potential μ and temperature to zero, one can show that, at low field, this paramagnetic Dirac susceptibility decays linearly from its zero-field value³⁸ as, $\chi_D(B) \cong \frac{\mu_0}{4\pi^2} \left[\frac{(g\mu_B)^2}{\hbar v_F} \Lambda - \frac{2(g\mu_B)^3}{\hbar^2 v_F^2} |B| + \dots \right]$. Where g is the Landé g -factor and Λ is the effective size of the momentum space contributing to the singular part of the free energy. It has been argued³⁸ that the maximum of the susceptibility, i.e., the peak height at zero field over the diamagnetic floor, depends on Λ , and thus controlled by the bulk bands. Whereas the nature of the singularity (i.e. cuspleness and linear-in-field decay of susceptibility at low fields, almost absence of thermal smearing, etc.) is universal to the entire family of 3D topological insulators. Inset of Fig. 4(b) shows the linear fit to the experimental data on the both sides of the zero-field cusp. The linear-in-field decay of the paramagnetic response, even at the highest measuring temperature 350 K, is evident from the figure.

Often, surface states show ageing effect, which has been attributed to surface reconstruction and the formation of two-dimensional electron gas due to the bending of the bulk band at the surface^{38–41}. To see whether such

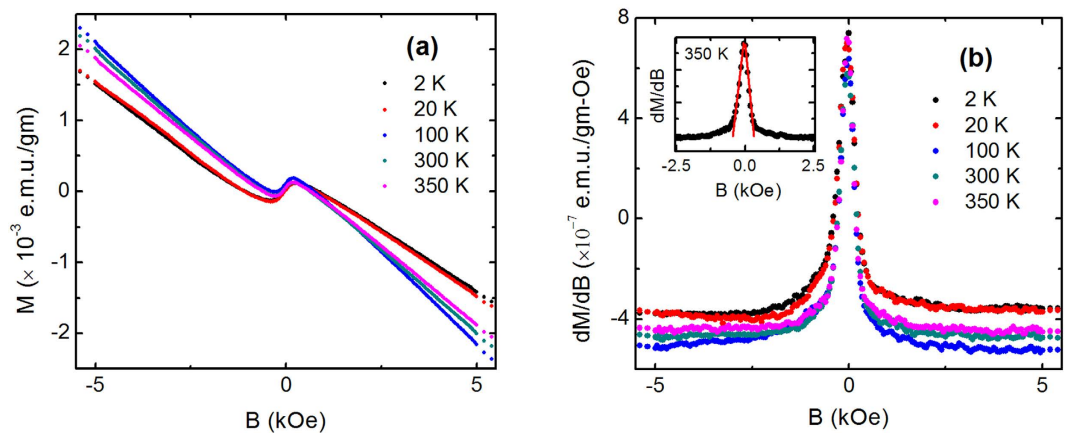


Figure 4. (a) Magnetization of ZrTe₅ single crystal, measured at several representative temperatures from 2 to 350 K. (b) Differential susceptibility ($\chi = \frac{dM}{dB}$) obtained after taking derivative of the magnetization with respect to external magnetic field. Inset shows the linear B dependence of χ , as B tending towards zero on both side of the zero field cusp at representative temperature 350 K.

behaviour is visible in the present case, similar measurements have been done on the same pieces of single crystals after three weeks of the first measurement [See Supplementary Figure S6]. Although the nature of the peak and its robustness against temperature remain unaffected, the reduction in peak height over time may be attributed to the expected ageing effect, similar to that observed in Bi₂Se₃, Sb₂Te₃ and Bi₂Te₃³⁸. It has been pointed out that the spin/orbit texture may also exist in the bulk state of the material with strong spin-orbit coupling, such as in BiTeI⁴² and WTe₂⁴³. Keeping this information in mind, one may think the possibility of the singular paramagnetic response from the bulk of ZrTe₅. But, as reported by the earlier ARPES measurements^{4,14,21}, the bulk state of ZrTe₅ holds a band gap ($\sim 50 \pm 10$ meV) between the upper and lower Dirac cone, which disobeys the primary condition for the singularity in electron spin orientation from the spin/orbit texture. Secondly, the negative longitudinal magnetoresistance due to chiral charge imbalance under non-trivial gauge field and ARPES results, established the presence of four-component massless Dirac fermion in the bulk 3D Dirac cone state of ZrTe₅. As far as we know, a four-component 3D Dirac fermion originating from the spin-degenerate band, cannot have any spin-orbit texture. The age dependent reduction of the peak height, whereas the diamagnetic background is unaffected, also confirms the surface origin of this singular paramagnetic response.

Discussion

We have detected a robust zero-field paramagnetic peak in the susceptibility of ZrTe₅ due to the helical spin texture associated with the Dirac fermions of the surface state of the three-dimensional topological insulator. Also, the negative longitudinal magnetoresistance implies induced chiral anomaly in ZrTe₅, which is the signature of the three-dimensional Dirac fermion in the bulk. This allows one to conclude that ZrTe₅ is a novel quantum phase of matter, which hosts both topological Dirac fermions on the surface and three-dimensional Dirac cone state with a mass gap between valence and conduction bands in the bulk. As mentioned earlier, ZrTe₅ can be either a weak or a strong three-dimensional topological insulator depending on the values of the lattice parameters¹². The simplest kind of topological insulator in three-dimension can be understood by stacking the layers of the 2D quantum spin Hall insulator with weak van der Waals bonding between them⁴⁴, similar to the stacking of monolayers of ZrTe₅ along **b** axis. A schematic diagram has been shown in Fig. 5, representing the possible minimum nontrivial electronic state in ZrTe₅ single crystal. Blue arrows represent the conducting edge state of a monolayer, which together form a topological surface state in the bulk sample. On the other hand, the bulk band with semiconducting gap is linear enough to show the signature of massless Dirac fermionic excitation in electronic transport.

In condensed matter electronic system, the topological classes are defined on the basis of the elementary concept, which states that the Hamiltonian cannot be smoothly deformed from one class of materials to another without closing the gap in electronic band structure. As a result, at the interface of the two materials with different topological band gap, there should be a conducting surface state, defined by the TKNN number^{44,45}. Unless there is a bulk gap, there should be no well-defined topological surface state. So, either band crossing in the bulk, i.e., 3D Dirac node or the 2D Dirac cone surface state can survive. In all 3D topological insulators reported so far, the semiconducting bulk band is highly non-linear and the gap is significantly large (~ 300 meV) compared to ZrTe₅^{38,46,47}. That is why the coexistence of 2D Dirac cone surface state and 3D Dirac fermions in the bulk is difficult. To the best of our knowledge, ZrTe₅ is the only 3D topological insulator in the history of material science, which has Dirac fermionic excitation in the bulk.

Note added. After completion of the present work [arXiv:1603.05175], we come across the results of ref. 19. From the scanning tunneling microscopy and angle-resolved photoemission spectroscopy, it has been shown that the monolayer of ZrTe₅ is a large gap 2D topological insulator, as the theory proposed¹². The authors have found conducting state at monolayer step edge of **ac**-plane and far away from the edge, i.e., well inside the plane,

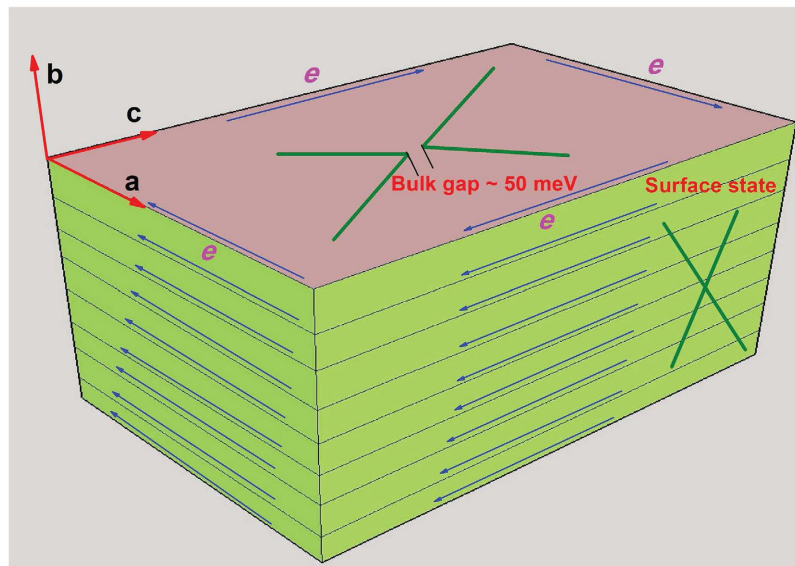


Figure 5. A schematic diagram, representing the minimum nontrivial topological nature of the electronic band structure of ZrTe_5 single crystal. ZrTe_5 monolayers, which lie in the ac -plane, stack together along the b -axis by weak van der Waals attraction. Independent conducting edge state of monolayers, as shown by the blue arrows in the figure, forms a topological surface state in bulk sample, known as weak three-dimensional topological insulating state.

the spectrum is fully gapped. This is consistent with our proposed nontrivial electronic state for the bulk ZrTe_5 , as shown in schematic Fig. 5. Very recently our results have been confirmed by Manzoni *et al.* through ARPES¹⁸.

Methods

A stoichiometric mixture of Zr (Alfa Aesar 99.9%) and Te (Alfa Aesar 99.99%) was sealed in a 15 cm long quartz tube with iodine (~5 mg/cc) and placed in a box furnace. It was then heated for seven days at 520 °C and cooled to room temperature at 10 °C/h. Next, the tube was shifted to a two-zone gradient furnace. One end of the tube containing the product was placed at 540 °C while the other end of the tube was placed at the cooler end of the furnace at 450 °C to provide a temperature gradient for four days. After slowly cooling (~30 °C/h) it to room temperature, single crystals with needlelike morphology were obtained at the cooler end.

The resistivity measurements were done by standard four-probe technique. Electrical contacts were made using conductive silver paste. The electrical transport measurements were carried out in 9 T physical property measurement system (Quantum Design) and cryogen free measurement system (Cryogenic). Magnetization was measured using a Superconducting Quantum Interference Device–Vibrating Sample Magnetometer (SQUID-VSM) (Quantum Design). Before the magnetization measurements, the system was standardized using single crystal of diamagnetic bismuth (Alfa Aesar 99.99%) and paramagnetic palladium [see Supplementary Figure 3 and Supplementary Figure 4(a)].

References

1. Furuseth, S., Brattas, L. & Kjekshus, A. The Crystal Structure of HfTe_5 . *Acta Chem. Scand.* **27**, 2367–2374 (1973).
2. Skelton, E. F. *et al.* Giant resistivity and X-ray diffraction anomalies in low-dimensional ZrTe_5 and HfTe_5 . *Solid State Communications.* **42**, 1–3 (1982).
3. Okada, S., Sambongi, T. & Ido, M. Giant Resistivity Anomaly in ZrTe_5 . *J. Phys. Soc. Jpn.* **49**, 839–840 (1980).
4. Li, Q. *et al.* Chiral magnetic effect in ZrTe_5 . *Nat. Phys.* **12**, 550–554 (2016).
5. Chen, R. Y. *et al.* Optical spectroscopy study of the three-dimensional Dirac semimetal ZrTe_5 . *Phys. Rev. B* **92**, 075107 (2015).
6. Jones, T. E., Fuller, W. W., Wieting, T. J. & Levy, F. Thermoelectric power of HfTe_5 and ZrTe_5 . *Solid State Commun.* **42**, 793–798 (1982).
7. Izumi, M., Uchinokura, K., Matsuura, E. & Harada, S. Hall effect and transverse magnetoresistance in a low-dimensional conductor HfTe_5 . *Solid State Commun.* **42**, 773–778 (1982).
8. Ong, N. P. & Monceau, P. Anomalous transport properties of a linear-chain metal: NbSe_3 . *Phys. Rev. B* **16**, 3443 (1977).
9. Okada, S. *et al.* Negative Evidences for Charge/Spin Density Wave in ZrTe_5 . *J. Phys. Soc. Jpn.* **51**, 460–467 (1982).
10. Rubinstein, M. HfTe_5 and ZrTe_5 : Possible polaronic conductors. *Phys. Rev. B* **60**, 1627 (1999).
11. McIlroy, D. N. *et al.* Observation of a semimetal semiconductor phase transition in the intermetallic ZrTe_5 . *J. Phys.: Condens. Matter* **16**, L359–L365 (2004).
12. Weng, H., Dai, X. & Fang, Z. Transition-Metal Pentatelluride ZrTe_5 and HfTe_5 : A Paradigm for Large-Gap Quantum Spin Hall Insulators. *Phys. Rev. X* **4**, 011002 (2014).
13. Tritt, T. M. *et al.* Large enhancement of the resistive anomaly in the pentatelluride materials HfTe_5 and ZrTe_5 with applied magnetic field. *Phys. Rev. B* **60**, 7816 (1999).
14. Manzoni, G. *et al.* Ultrafast Optical Control of the Electronic Properties of ZrTe_5 . *Phys. Rev. Lett.* **115**, 207402 (2015).
15. Chen, R. Y. *et al.* Magnetoinfrared Spectroscopy of Landau Levels and Zeeman Splitting of Three-Dimensional Massless Dirac Fermions in ZrTe_5 . *Phys. Rev. Lett.* **115**, 176404 (2015).
16. Zhou, Y. *et al.* Pressure-induced semimetal to superconductor transition in a three-dimensional topological material ZrTe_5 . *Proc. Natl. Acad. Sci. USA* **113**(11), 2904–2909 (2016).

17. Yuan, X. *et al.* Observation of quasi-two-dimensional Dirac fermions in ZrTe₅. *NPG Asia Materials* **8**, e325 (2016).
18. Niu, J. *et al.* Electrical transport in nano-thick ZrTe₅ sheets: from three to two dimensions. Preprint at <https://arxiv.org/abs/1511.09315> (2015).
19. Wu, R. *et al.* Experimental evidence of large-gap two-dimensional topological insulator on the surface of ZrTe₅. *Phys. Rev. X* **6**, 021017 (2016).
20. Yu, W. *et al.* Quantum Oscillations at Integer and Fractional Landau Level Indices in ZrTe₅. Preprint at <https://arxiv.org/abs/1602.06824> (2016).
21. Zhang, Y. *et al.* Electronic Evidence of Temperature-Induced Lifshitz Transition and Topological nature in ZrTe₅. Preprint at <https://arxiv.org/abs/1602.03576> (2016).
22. DiSalvo, F. J., Fleming, R. M. & Waszczak, J. V. Possible phase transition in the quasi-one-dimensional materials ZrTe₅ or HfTe₅. *Phys. Rev. B* **24**, 2935 (1981).
23. Fjellvåg, H. & Kjekshus, A. Structural properties of ZrTe₅ and HfTe₅ as seen by powder diffraction. *Solid State Commun.* **60**, 91–93 (1986).
24. Okada, S., Sambongi, T. & Ido, M. Giant Resistivity Anomaly in ZrTe₅. *J. Phys. Soc. Jpn.* **49**, 839 (1980).
25. Littleton IV, R. T. *et al.* Suppression of the resistivity anomaly and corresponding thermopower behavior in the pentatelluride system by the addition of Sb: Hf_{1-x}Zr_xTe_{5-y}Sb_y. *Phys. Rev. B* **64**, 121104(R) (2001).
26. Izumi, M. *et al.* Shubnikov-de Haas oscillations and Fermi surfaces in transition-metal pentatellurides ZrTe₅ and HfTe₅. *J. Phys. C: Solid State Phys.* **20**, 3691 (1987).
27. Adler, S. L. Axial-Vector Vertex in Spinor Electrodynamics. *Phys. Rev.* **177**, 2426 (1969).
28. Bell, J. S. & Jackiw, R. A PCAC puzzle: $\pi^0 \rightarrow \gamma\gamma$ in the σ -model. *Il Nuovo Cimento A* **60**, 47–61 (1969).
29. Nielsen, H. B. & Ninomiya, M. The Adler-Bell-Jackiw anomaly and Weyl fermions in a crystal. *Phys. Lett. B* **130**, 389–396 (1983).
30. Gorbar, E. V., Miransky, V. A. & Shovkovy, I. A. Engineering Weyl nodes in Dirac semimetals by a magnetic field. *Phys. Rev. B* **88**, 165105 (2013).
31. Li, C. Z. *et al.* Giant negative magnetoresistance induced by the chiral anomaly in individual Cd₃As₂ nanowires. *Nat. Commun.* **6**, 10137 (2015).
32. Kim, H.-J. *et al.* Dirac versus Weyl Fermions in Topological Insulators: Adler-Bell-Jackiw Anomaly in Transport Phenomena. *Phys. Rev. Lett.* **111**, 246603 (2013).
33. Huang, X. *et al.* Observation of the Chiral-Anomaly-Induced Negative Magnetoresistance in 3D Weyl Semimetal TaAs. *Phys. Rev. X* **5**, 031023 (2015).
34. Zheng, G. *et al.* Transport evidence for the three-dimensional Dirac semimetal phase in ZrTe₅. *Phys. Rev. B* **93**, 115414 (2016).
35. Xiong, J. *et al.* Evidence for the chiral anomaly in the Dirac semimetal Na₃Bi. *Science* **350**, 413 (2015).
36. Hsieh, D. *et al.* A tunable topological insulator in the spin helical Dirac transport regime. *Nature* **460**, 1101 (2009).
37. Zhang, H., Liu, C.-X. & Zhang, S.-C. Spin-Orbital Texture in Topological Insulators. *Phys. Rev. Lett.* **111**, 066801 (2013).
38. Zhao, L. *et al.* Singular robust room-temperature spin response from topological Dirac fermions. *Nat. Mater.* **13**, 580 (2014).
39. Buga, S. G. *et al.* Superconductivity in bulk polycrystalline metastable phases of Sb₂Te₃ and Bi₂Te₃ quenched after high-pressure-high-temperature treatment. *Chem. Phys. Lett.* **631–632**, 97 (2015).
40. He, X. *et al.* Surface Termination of Cleaved Bi₂Se₃, Investigated by Low Energy Ion Scattering. *Phys. Rev. Lett.* **110**, 156101(2013).
41. Bahramy, M. S. *et al.* Emergent quantum confinement at topological insulator surfaces. *Nat. Commun.* **3**, 1159 (2012).
42. Murakawa, H. *et al.* Detection of Berry's Phase in a Bulk Rashba Semiconductor. *Science* **342**, 1490 (2013).
43. Jiang, J. *et al.* Signature of Strong Spin-Orbital Coupling in the Large Nonsaturating Magnetoresistance Material WTe₂. *Phys. Rev. Lett.* **115**, 166601 (2015).
44. Hasan, M. Z. & Kane, C. L. Colloquium: Topological insulators. *Rev. Mod. Phys.* **82**, 3045 (2010).
45. Kitaev, A. Periodic table for topological insulators and superconductors. *AIP Conf. Proc.* **1134**, 22 (2009).
46. Yan, B., Jansen, M. & Felser, C. A large-energy-gap oxide topological insulator based on the superconductor BaBiO₃. *Nat. Phys.* **9**, 709711 (2013).
47. Yan, B. & Zhang, S.-C. Topological materials. *Rep. Prog. Phys.* **75**, 096501 (2012).
48. Manzoni, G. *et al.* Evidence for a Strong Topological Insulator Phase in ZrTe₅. Preprint at <https://arxiv.org/abs/1608.03433> (2016).

Acknowledgements

We thank V.A. Kulbachinskii for useful discussions.

Author Contributions

A.P. prepared the sample. A.P. performed the experiments. A.P. and P.M. analysed and interpreted the data. A.P. and P.M. wrote the paper. P.M. supervised the project.

Additional Information

Supplementary information accompanies this paper at <http://www.nature.com/srep>

Competing financial interests: The authors declare no competing financial interests.

How to cite this article: Pariari, A. and Mandal, P. Coexistence of topological Dirac fermions on the surface and three-dimensional Dirac cone state in the bulk of ZrTe₅ single crystal. *Sci. Rep.* **7**, 40327; doi: 10.1038/srep40327 (2017).

Publisher's note: Springer Nature remains neutral with regard to jurisdictional claims in published maps and institutional affiliations.



This work is licensed under a Creative Commons Attribution 4.0 International License. The images or other third party material in this article are included in the article's Creative Commons license, unless indicated otherwise in the credit line; if the material is not included under the Creative Commons license, users will need to obtain permission from the license holder to reproduce the material. To view a copy of this license, visit <http://creativecommons.org/licenses/by/4.0/>

© The Author(s) 2017